

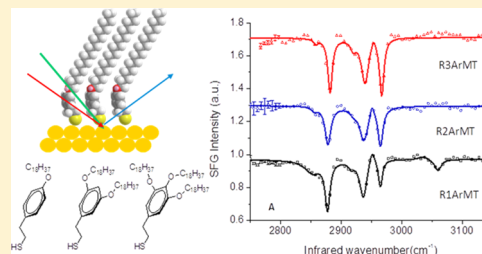
# Characterization of SAMs Derived from Octadecyloxyphenylethanethiols by Sum Frequency Generation

Jack Deodato C. Jacob, Supachai Rittikulsittichai, T. Randall Lee,\* and Steven Baldelli\*

Department of Chemistry, University of Houston, Houston, Texas 77204–5003

**ABSTRACT:** Sum frequency generation (SFG) vibrational spectroscopy analyses were performed on self-assembled monolayers (SAMs) formed via the adsorption of 2-(4(octadecyloxy)phenylethanethiol (**R1ArMT**), 2-(3,5-bis(octadecyloxy)phenylethanethiol (**R2ArMT**), and 2-(3,4,5-tris(octadecyloxy)phenylethanethiol (**R3ArMT**) on gold. SFG spectra showed that the monolayers formed were closely packed and well ordered. It was determined, using orientation analysis, that as additional octadecyloxy chains were attached to the aromatic ring the apparent methyl group tilt increased and conformational order decreased. Aromatic C–H modes exhibited in the SFG spectra suggest the aromatic rings have a  $C_2$  axis along the surface normal.

Model phenylethanethiols with different symmetries along the benzene ring were synthesized and used to identify vibrational modes and the surface orientation of the alkoxyphenylethanethiols. SAMs derived from **R1ArMT** exhibit aromatic C–H stretching modes due to the  $C_{2v}$  symmetry at the ring. In contrast, SAMs derived from **R2ArMT** and **R3ArMT** exhibit no aromatic C–H stretching modes due to their low Raman cross section.



## 1. INTRODUCTION

SAMs are organized layers of organic molecules spontaneously adsorbed onto the surface of solids. These molecules can be tailored by varying headgroups,<sup>1–5</sup> end groups,<sup>6–13</sup> and spacers<sup>14</sup> to change the wetting and interfacial properties of the resultant monolayer for various applications.<sup>15</sup> Many SAMs systems have been studied, and most investigations have concentrated on gold as the substrate because of its inertness to form oxides, its resistance to atmospheric contamination, and its strong chemical affinity to sulfur headgroups.<sup>16</sup>

Alkanethiolate SAMs are created by the chemisorption of hydrophilic “headgroups” onto a substrate from either the vapor or liquid phase, followed by a slow 2-D organization of the hydrophobic “tail groups”.<sup>17</sup> After the organizational step, long chain alkanethiols assume a well-ordered and densely packed monolayer<sup>18</sup> that can act as a nanoscale protective barrier on metals against corrosive agents. Given their dense packing and their ease of preparation, SAMs are attractive for use in corrosion inhibition.

One drawback of SAMs is their instability; in particular, they can be removed by exposure to elevated temperature, displacement by other molecules, and mechanical stress. One strategy to enhance stability is to establish multiple anchor points between the substrate and the molecules of the monolayer. Multidentate thiols,<sup>3,19</sup> having multiple thiol moieties within a headgroup, show promise with their increased thermal stability but exhibit decreased conformational order due to steric hindrances. In recent efforts to address this shortcoming, a family of alkoxyphenylethanethiols (Figure 1) having terminal mono-(**R1ArMT**), di-(**R2ArMT**), and tri-(**R3ArMT**) octadecyloxy chains was developed, and their self-assembly on gold was examined.<sup>20</sup> On the basis of previous investigations,<sup>21</sup> we hypothesized that the octadecyl com-

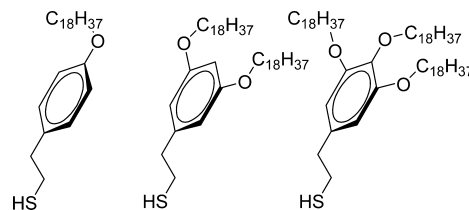


**Figure 1.** Thiols analyzed in this study. From left to right: 2-(4(octadecyloxy)phenylethanethiol (**R1ArMT**), 2-(3,5-bis(octadecyloxy)phenylethanethiol (**R2ArMT**), and 2-(3,4,5-tris(octadecyloxy)phenylethanethiol (**R3ArMT**).

ponents of these thiols would form well-ordered monolayers similar to long-chain alkanethiols, while the aromatic ring in future analogs could provide several points of attachment for multidentate binding.

In the present study, SAMs derived from these alkoxyphenylethanethiols were probed using sum frequency generation (SFG) spectroscopy, and their SFG spectra were used to determine the order and the orientation of the adsorbates on the surface of gold. Model phenylethanethiols were synthesized and analyzed to determine the effect of these factors on the SFG intensity of the aromatic C–H stretching modes: (1) the symmetry along the benzene ring and (2) the presence of long alkoxy chains on the ring.

**Received:** March 6, 2013

**Revised:** April 3, 2013

**Published:** April 29, 2013

Table 1. Fresnel Coefficients for Gold/Air Interface

|                             | $K_{xx}$       | $K_{yy}$        | $K_{zz}$        |
|-----------------------------|----------------|-----------------|-----------------|
| IR (2980 $\text{cm}^{-1}$ ) | 0.017 – 0.091i | 0.006 – 0.0462i | 0.793 + 0.0731i |
| visible (532 nm)            | 0.432 – 0.487i | 0.185 – 0.430i  | 0.474 + 0.270i  |
| SFG (459 nm)                | 0.493 – 0.278i | 0.322 – 0.320i  | 0.440 + 0.161i  |

## 2. BACKGROUND

**Sum Frequency Generation Spectroscopy.** SFG is a second-order nonlinear optical technique that is inherently surface-sensitive, making it an excellent technique in analyzing monolayers. SFGn occurs when a visible laser and a tunable infrared (IR) laser are pulsed simultaneously on a surface.<sup>22,23</sup> When the IR beam is tuned through a vibrational resonance of the adsorbate, it induces a vibrational transition from the ground state to an excited state. The visible beam simultaneously induces a transition to a higher energy virtual state similar to an antistokes Raman process to produce the coherent SFG beam.

The intensity of the SFG beam,  $I_{\text{SFG}}$ , is directly proportional to the square of the second-order polarizability, which is expressed as shown in eqs 1 and 2, where  $\chi_{\text{NR}}^{(2)}$  is the nonresonant susceptibility arising from the gold substrate, while  $\chi_{\text{R}}^{(2)}$  contains the vibrational information of the molecules on the surface.

$$I_{\text{SFG}} \propto |\chi_{\text{R}}^{(2)} + \chi_{\text{NR}}^{(2)}|^2 = \left| \sum \frac{A_q}{\omega_{\text{IR}} - \omega_q - i\Gamma} + \chi_{\text{NR}}^{(2)} \right|^2 \quad (1)$$

$$\begin{aligned} \chi^{(2)} &= \chi_{\text{R}}^{(2)} + \chi_{\text{NR}}^{(2)} \\ &= |\chi_{\text{R}}^{(2)}|^2 + |\chi_{\text{NR}}^{(2)}|^2 + 2|\chi_{\text{R}}^{(2)}||\chi_{\text{NR}}^{(2)}| \cos[\varepsilon - \delta(\omega_{\text{IR}})] \end{aligned} \quad (2)$$

Notably,  $\chi_{\text{R}}^{(2)}$  is proportional to the average hyperpolarizability of the adsorbate,  $\beta^{(2)}$ , which, in turn, is proportional to the product of the IR and Raman transition moments, as shown in eq 3. Thus, molecular vibrations will only be SFG-active if they are IR-active and Raman-active. In the electric dipole approximation, SFG only occurs in noncentrosymmetric crystals or at the interface, since Raman and IR transitions are exclusive in centrosymmetric media.

$$\chi_{\text{R}}^{(2)} \propto N\langle\beta^{(2)}\rangle \quad (3)$$

Monolayers that are isotropic in the plane of the surface have only four combinations of polarizations that allow sum frequency emission:  $\chi_{ijk}^{(2)}$ :  $\chi_{zxx}^{(2)} = \chi_{zyy}^{(2)}$ ,  $\chi_{xzx}^{(2)} = \chi_{yzy}^{(2)}$ ,  $\chi_{xxz}^{(2)} = \chi_{yyz}^{(2)}$ , and  $\chi_{zzz}^{(2)}$  and can be probed using the following polarizations:

$$I_{\text{ssp}} \approx |\chi_{yyz}^{(2)}| : E_{\text{vis}}E_{\text{IR}}|^2$$

$$I_{\text{sps}} \approx |\chi_{zyy}^{(2)}| : E_{\text{vis}}E_{\text{IR}}|^2$$

$$I_{\text{pss}} \approx |\chi_{zzy}^{(2)}| : E_{\text{vis}}E_{\text{IR}}|^2$$

$$\begin{aligned} I_{\text{ppp}} \approx & |\chi_{zzz}^{(2)}| : E_{\text{vis}}E_{\text{IR}} + \chi_{zxx}^{(2)} : E_{\text{vis}}E_{\text{IR}} + \chi_{xxz}^{(2)} \\ & : E_{\text{vis}}E_{\text{IR}} + \chi_{xzx}^{(2)} : E_{\text{vis}}E_{\text{IR}}|^2 \end{aligned}$$

Here  $\chi_{ijk}^{(2)}$  is the second-order nonlinear surface susceptibility and  $i,j,k$  are the laboratory coordinates at the interface. For monolayers on metal surfaces such as gold, copper, or silver, the Fresnel coefficients of the  $z$  component of the IR electric field at the surface are much larger than the  $x$  and  $y$  components (Table 1). Thus, on gold, sum frequency emission is dominated by polarization combinations with a  $z$  component of the IR electric field, namely, ssp and ppp.<sup>24</sup> On metal surfaces where  $\chi_{\text{NR}}^{(2)}$  is much larger than the  $\chi_{\text{R}}^{(2)}$ , the cross term in eq 3 is the main contributor of the ppp spectra of the adsorbates.<sup>25,26</sup> The SFG spectra in this study were fitted using eq 2, where  $A_q$ ,  $\omega_{\text{IR}}$ ,  $\omega_q$ , and  $\Gamma$  are the amplitude, IR laser frequency, vibrational transition frequency, and the damping constant, respectively.

In addition to SFG spectroscopy, which samples the average SFG spectra of a 1 mm area on the surface, the SAMs were also analyzed by SFG imaging microscopy. This microscope can be used to characterize the spatial and chemical nature of molecules on a surface and is an excellent technique in chemical imaging, to supplement the SFG spectroscopy technique by providing both structural and orientational details. In addition, distribution analysis of the SFG images can provide information regarding the conformational order of the SAMs.

## 3. EXPERIMENTAL SECTION

**3.1. Materials.** Octadecanethiol (ODT, Sigma), heptadecanethiol (C17, Sigma), and 2-phenylethanethiol (PET, Sigma) were used as received without further purification. The syntheses of R1ArMT, R2ArMT, and R3ArMT are described elsewhere.<sup>20</sup> The compounds 2-(4-methoxyphenyl)ethanethiol (MET), 2-*p*-tolylethanethiol (TET), 2-(3,4-dimethoxyphenyl)ethanethiol (3,4-DMP), and 2-(3,5-dimethoxyphenyl)ethanethiol (3,5-DMP) were synthesized from their bromide precursors (Sigma) via thioacetate substitution and then deprotection using lithium aluminum hydride ( $\text{LiAlH}_4$ ).

**3.2. Preparation of SAMs.** Gold substrates were prepared by the thermal evaporation of gold onto chromium-primed silicon wafers at a rate of 1 Å/s in a chamber equipped with a diffusion pump at high vacuum pressure of  $10^{-6}$  Torr. After the deposition of 1000 Å of gold, the chamber was cooled to room temperature and flushed with ultrapure nitrogen gas. The gold slides were immersed in 1 mM thiol solutions (THF) and allowed to equilibrate for a period of 72 h. The resultant SAMs were thoroughly rinsed with THF and ethanol and then blown dry with ultrapure nitrogen before characterization in air.

**3.3. Analysis and Treatment of Data: SFG Spectroscopy.** The SFG spectrometer used in the experiments has been described elsewhere.<sup>27</sup> An EKSPPLA PL-2251A Nd:YAG laser at 1064 nm with a 19 ps long pulse and a 20 Hz repetition rate was used as the pump source. The optical parametric generation/optical parametric amplification (OPG/OPA) (LaserVision) system generates a tunable IR beam from 2000 to 4000  $\text{cm}^{-1}$ . The visible 532 nm beam was produced by doubling the frequency of the 1064 nm beam via a KTP crystal. The visible and IR beams, adopting a copropagating configuration in which incidence angles of the visible and IR beams are 50 and 60°, respectively, were spatially and

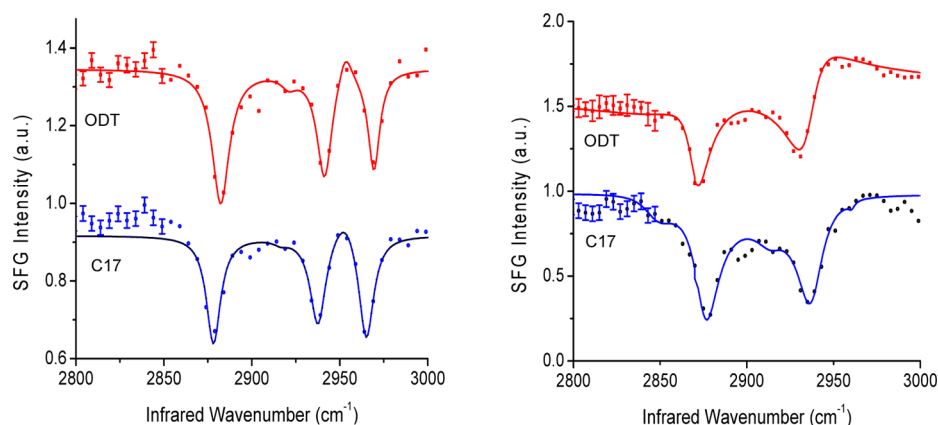


**Figure 2.** SFG spectra of SAMs derived from  $\text{CH}_3(\text{CH}_2)_{17}\text{SH}$  (ODT) and  $\text{CH}_3(\text{CH}_2)_{16}\text{SH}$  (C17) on gold in the CH region (A) ppp and (B) ssp polarization configuration. The ODT spectra are offset by 0.8 for clarity.

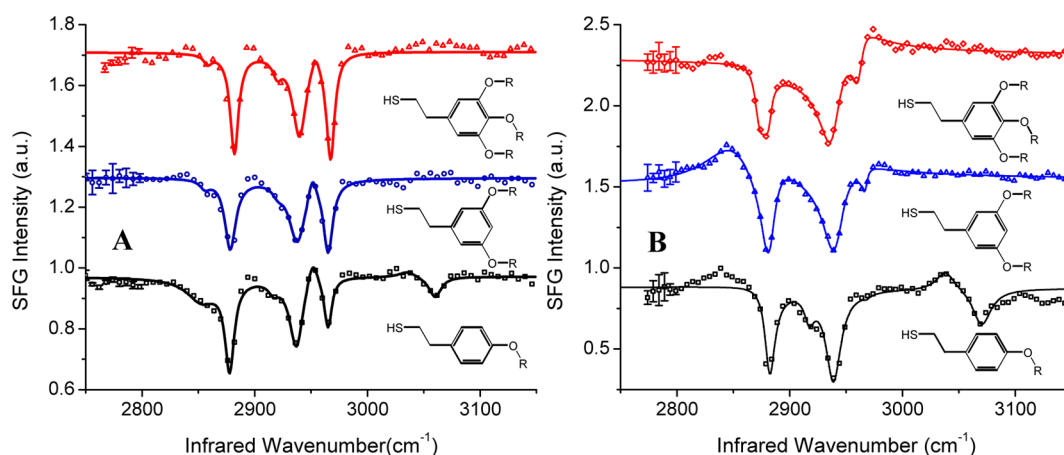


**Figure 3.** SFG spectra of R1ArMT, R2ArMT, and R3ArMT SAMs on gold in the CH region (A) ppp and (B) ssp polarization configuration. Spectrum was offset by 0.3 for clarity.  $\text{R} = \text{CH}_3(\text{CH}_2)_{17}$ .

temporally overlapped at the surface to produce an SFG signal. The SFG beam was passed through an interference filter and a monochromator to eliminate scattered light and collected with a photomultiplier tube (PMT). Two polarization combinations, ssp (s-polarized SFG, s-polarized visible beam, and p-polarized IR beam) and ppp, were acquired in the C–H stretching region from 2750 to 3150  $\text{cm}^{-1}$  for each sample. The scan rate was 1  $\text{cm}^{-1}/\text{s}$  with an average of 20 laser shots per data point. Each spectrum is an average of five or more scans. Each SFG spectrum was fitted in Mathematica 8 using a nonlinear curve-fitting function using eq 2.

**3.4. SFG-Imaging Microscopy (SFG-IM).** The SFG imaging microscope uses the same laser source as the system described above but utilizes the 1064 nm fundamental and the tunable IR beam at incident angles of  $60^\circ$  and  $70^\circ$  from the surface normal, respectively, to produce the SFG signal. The SFG-imaging microscopy (SFG-IM) uses a ppp polarization configuration and offers a spatial resolution of 2  $\mu\text{m}$ .<sup>28</sup>

Data were collected by tuning the IR beam at a constant rate and averaging the SFG signal in 5  $\text{cm}^{-1}$  intervals with 3000 shots per data point.<sup>29</sup> A  $400 \times 400 \mu\text{m}^2$  pixel area image of the surface was divided into  $10 \times 10$  squares, producing 1600 regions. The spectra of these regions were individually extracted with ImageJ<sup>30</sup> and fitted using Mathematica 8.

For tilt-angle analysis, the ratios of the methyl symmetric and antisymmetric modes ( $r^+/r^-$ ) were compared with the bond

polarizability model.<sup>31–33</sup> The ratios of the  $\text{CH}_2/\text{CH}_3$  were used to analyze gauche defects. The results were then remapped into contour plots to show the spatial distribution of the ratios.

## 4. RESULTS AND DISCUSSION

**4.1. SFG Spectra.** Because of the colinear configuration of the SFG instrument, the nonresonant signal of the gold substrate has a phase opposite that of the monolayer. When the molecules are in resonance, a destructive interference occurs, producing dips instead of peaks. Given this background, the SFG spectra of SAMs derived from ODT and C17 are shown in Figure 2. The observed resonances can be assigned to the vibrations of the alkane chain of the alkanethiols: the  $\text{CH}_2$  symmetric stretch ( $d^+$ ) at 2850  $\text{cm}^{-1}$  and its Fermi resonance ( $d^{\text{FR}}$ ) at 2915  $\text{cm}^{-1}$ , the symmetric stretch of the  $\text{CH}_3$  group ( $r^+$ ) at 2870  $\text{cm}^{-1}$  and its Fermi resonance ( $r^{\text{FR}}$ ) at 2935  $\text{cm}^{-1}$ , and the  $\text{CH}_3$  antisymmetric out-of-plane and in-plane stretches ( $r^{\text{op}}$  and  $r^-$ ) at 2950 and 2965  $\text{cm}^{-1}$ , respectively.<sup>34–37</sup>

The SFG spectra of ODT and C17 are characteristic of densely packed and well-ordered monolayers on gold. Both spectra are dominated by strong dips attributed to the C–H stretching modes of the terminal methyl group. The near-absence of methylene C–H stretching modes at 2850 and 2915  $\text{cm}^{-1}$  indicates that both monolayers are well-ordered. In well-packed monolayers such as those formed by long-chain

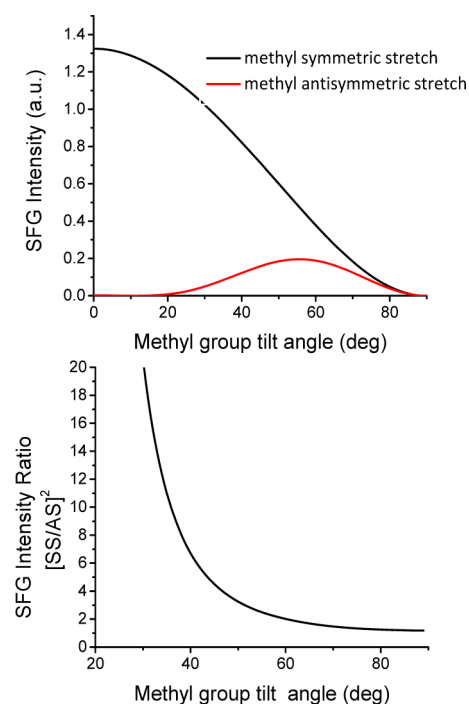


**Figure 4.** (top) Intensity of  $r^+$  and  $r^-$  versus methyl group tilt angle (ppp polarization). (bottom)  $r^+/r^-$  intensity ratio versus methyl group tilt angle.

**Table 2. Methyl Tilts of Analyzed Phenylalkanethiols**

|        | $r^+$         | $r^-$          | $r^+/r^-$      | methyl group tilt angle ( $\theta$ ) | range |
|--------|---------------|----------------|----------------|--------------------------------------|-------|
| ODT    | $2.9 \pm 0.1$ | $1.03 \pm 0.1$ | $2.85 \pm 0.1$ | 33.8                                 | 0.8   |
| C17    | $2.5 \pm 0.1$ | $2.03 \pm 0.1$ | $1.25 \pm 0.1$ | 55.9                                 | 4.9   |
| R1ArMT | $1.8 \pm 0.1$ | $0.68 \pm 0.1$ | $2.69 \pm 0.1$ | 34.8                                 | 1.0   |
| R2ArMT | $1.8 \pm 0.1$ | $0.83 \pm 0.1$ | $2.16 \pm 0.1$ | 39.2                                 | 1.5   |
| R3ArMT | $1.8 \pm 0.1$ | $1.14 \pm 0.1$ | $1.58 \pm 0.1$ | 47.2                                 | 2.7   |

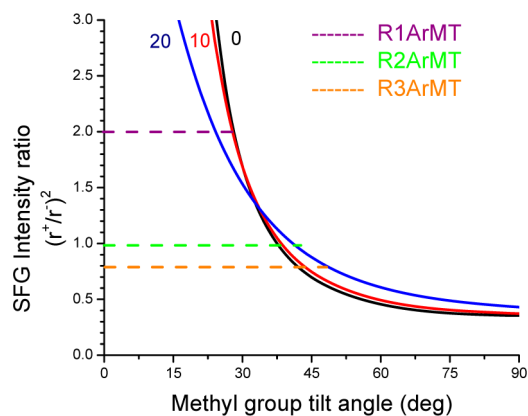


**Figure 5.** SFG-IM intensity ( $r^+/r^-$ ) ratio versus tilt angle. Each curve represents a different distribution width ( $\sigma$ , deg) where  $\sigma = 0^\circ$  is the  $\delta$  function distribution (black curve). The estimated tilt angles of the studied SAMs are also shown.

alkanethiols on gold, the alkyl chains assume an all-trans configuration. In this environment, the methylene modes have local centers of inversion and are therefore SFG-inactive.<sup>24,34</sup>

Figure 3 shows the ppp and ssp spectra of the phenyl-ethylthiol SAMs on gold in air. Specifically, Figure 3A shows

the ppp spectrum of R1ArMT, which exhibits strong resonances at 2878, 2938, 2950, and 2966  $\text{cm}^{-1}$  assigned as  $r^+$ ,  $r^{\text{FR}}$ ,  $r^{\text{op}}$ , and  $r^-$  modes of the terminal methyl group, respectively. Weak methylene modes  $d^+$  and  $d^{\text{FR}}$  appear at 2850 and 2915  $\text{cm}^{-1}$ . The broad dip at 3061  $\text{cm}^{-1}$  was assigned as the  $\nu_2$  aromatic C–H stretch using Wilson's nomenclature<sup>38</sup> (vide infra). The ssp spectrum of R1ArMT in Figure 3B features the methyl symmetric C–H stretch (2881  $\text{cm}^{-1}$ ) with its Fermi resonance (2939  $\text{cm}^{-1}$ ), and the  $\nu_2$  aromatic C–H stretch as a dip at 3068  $\text{cm}^{-1}$ . The resonance at 3037  $\text{cm}^{-1}$  was assigned as an aromatic C–H stretching mode  $\nu_7b$ .<sup>39</sup>

The ppp spectrum in Figure 3A of SAMs derived from R2ArMT shows dips attributed to the methyl group at 2877, 2936, 2950, and 2965  $\text{cm}^{-1}$  assigned as  $r^+$ ,  $r^{\text{FR}}$ ,  $r^{\text{op}}$ , and  $r^-$ , respectively. Methylene modes  $d^+$  and  $d^{\text{FR}}$  appear at 2850 and 2915  $\text{cm}^{-1}$ . It is similar to the R1ArMT spectrum, with the notable absence of the aromatic stretching mode at 3060  $\text{cm}^{-1}$ . Furthermore, the ssp spectrum in Figure 3B has dips at 2881, 2940, and 2966  $\text{cm}^{-1}$  assigned as  $r^+$ ,  $r^{\text{FR}}$ , and  $r^-$ , respectively. Similarly, the ppp spectrum in Figure 3A of SAMs derived from R3ArMT shows similar resonances as R2ArMT at 2881, 2940, 2950, and 2967  $\text{cm}^{-1}$ , assigned as  $r^+$ ,  $r^{\text{FR}}$ ,  $r^{\text{op}}$  and  $r^-$ , respectively. The ssp spectrum in Figure 3B has dips at 2878, 2935, and 2961  $\text{cm}^{-1}$  assigned as  $r^+$ ,  $r^{\text{FR}}$ , and  $r^-$ , respectively.

SAMs derived from R1ArMT, R2ArMT, and R3ArMT all exhibit SFG spectra similar to ODT and C17, with the methyl stretching modes in dominance, suggesting that these thiols form well-ordered monolayers on gold. However, weak methylene resonances for all of these new SAMs suggest the presence of some degree of disorder. Methylene CH stretching modes at 2848 and 2916  $\text{cm}^{-1}$  usually suggest minor gauche defects on the chains in the monolayers (e.g., from either pinhole defects or collapse sites).<sup>40</sup> However, in the case of these SAMs, the methylene modes might stem from kinks caused by having alkoxy groups attached to the phenyl ring.

The mismatch in the cross-sectional areas between the aromatic and the alkyl portions of these thiol adsorbates introduces a 10–25% void space in the monolayer, causing the methylene groups attached to the aromatic ring (up to five carbons) to compensate by kinking and bending until the methylene groups further up the chain align to form an all-trans configuration.<sup>41</sup> These kink defects introduce a noncentrosymmetric environment, causing the methylene groups to be SFG-active. However, the alkoxy chains of these adsorbates are of sufficient length to compensate for this void space such that the interface of the SAMs exhibits characteristics similar to a well-ordered monolayer, as shown in previous analyses.<sup>20</sup>

**4.2. Methyl Group Tilt.** The methyl group tilt can be estimated by deriving the  $r^+/r^-$  ratio. The symmetric and antisymmetric stretching modes of the methyl group are orthogonal, such that as the methyl group tilts away from the surface normal the intensity of the  $r^-$  mode increases while the  $r^+$  mode decreases (Figure 4). This relationship can be qualitatively observed in both ppp and ssp spectra of ODT and C17 (Figure 2). ODT possesses an even chain length, and SAMs derived from it exhibit a methyl tilt of  $\sim 35^\circ$ .<sup>42</sup> Its  $r^+$  intensity is considerably greater than its  $r^-$  intensity. The adsorbate C17, having an odd chain length, exhibits a methyl tilt of  $\sim 55^\circ$ , and its  $r^+/r^-$  ratio is greater than that of ODT. By comparing the ratio between the intensities of the symmetric and antisymmetric methyl stretches ( $r^+/r^-$ ) of the ppp spectra with a theoretical orientation curve (Figure 4), the tilt angle of the terminal methyl group can be approximated using the bond

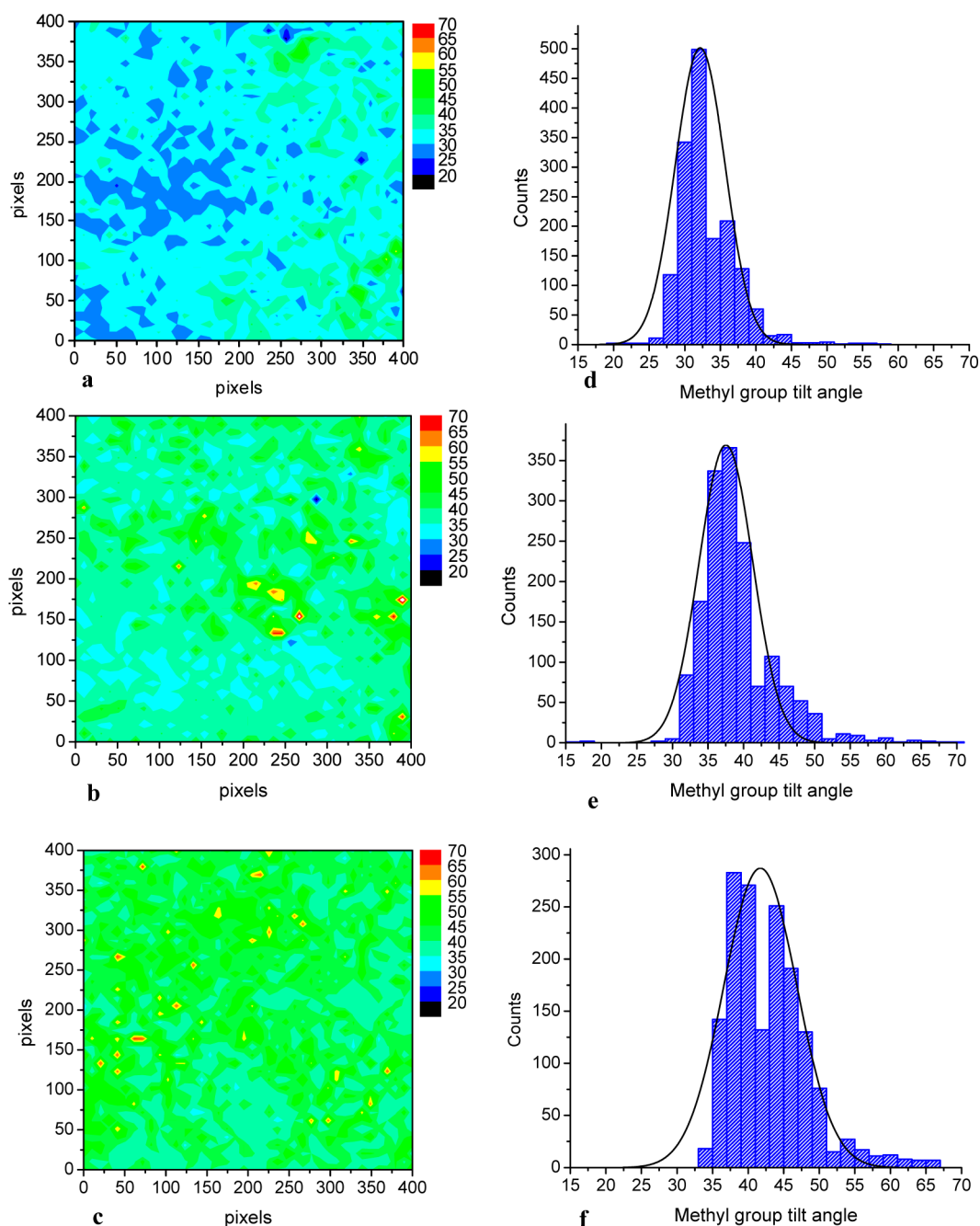


**Figure 6.** Contour plots of  $(r^+/r^-)$  ratio of SAMs derived from (a) R1ArMT, (b) R2ArMT, and (c) R3ArMT with their corresponding histogram plots (d–f, respectively).

**Table 3. Methyl Tilts Angles and  $\text{CH}_2/\text{CH}_3$  Ratio of Phenylalkanethiols on Gold**

| molecule | tilt angle (deg) | range (deg) | $\text{CH}_2/\text{CH}_3$ ratio | range |
|----------|------------------|-------------|---------------------------------|-------|
| R1ArMT   | 33               | 4           | 0.13                            | 0.09  |
| R2ArMT   | 39               | 6           | 0.24                            | 0.14  |
| R3ArMT   | 43               | 6           | 0.41                            | 0.16  |

polarizability model and calculations done by Wang and coworkers<sup>33</sup> and by Hirose and coworkers.<sup>31,32</sup> Table 2 shows the methyl tilts of the SAMs derived from Figure 4. The adsorbates ODT and C17 were also included as references. The methyl group tilts of the phenylethanethiols follow the trend: R1ArMT < R2ArMT < R3ArMT. The increased number of

alkoxy chains attached to a phenyl ring might cause steric repulsions that decrease the conformational order of the monolayer and increase the tilt of the chains.<sup>43</sup> Alternatively, the positions where the alkoxy chains are attached to the ring might also contribute to the methyl group tilt. The alkoxy chain of R1ArMT is connected to the para position of the ring, while the R2ArMT alkoxy chains are anchored at the meta positions. These two positions on the ring have dissimilar heights and angles in relation to the surface normal and might affect the tilt of the terminal methyl groups. It is also important to note that the measured methyl tilt angles are the average of all of the methyl groups on the surface.

**4.3. Chemical Imaging and Distribution Analysis.** To gain an even better understanding of the chemical morphology

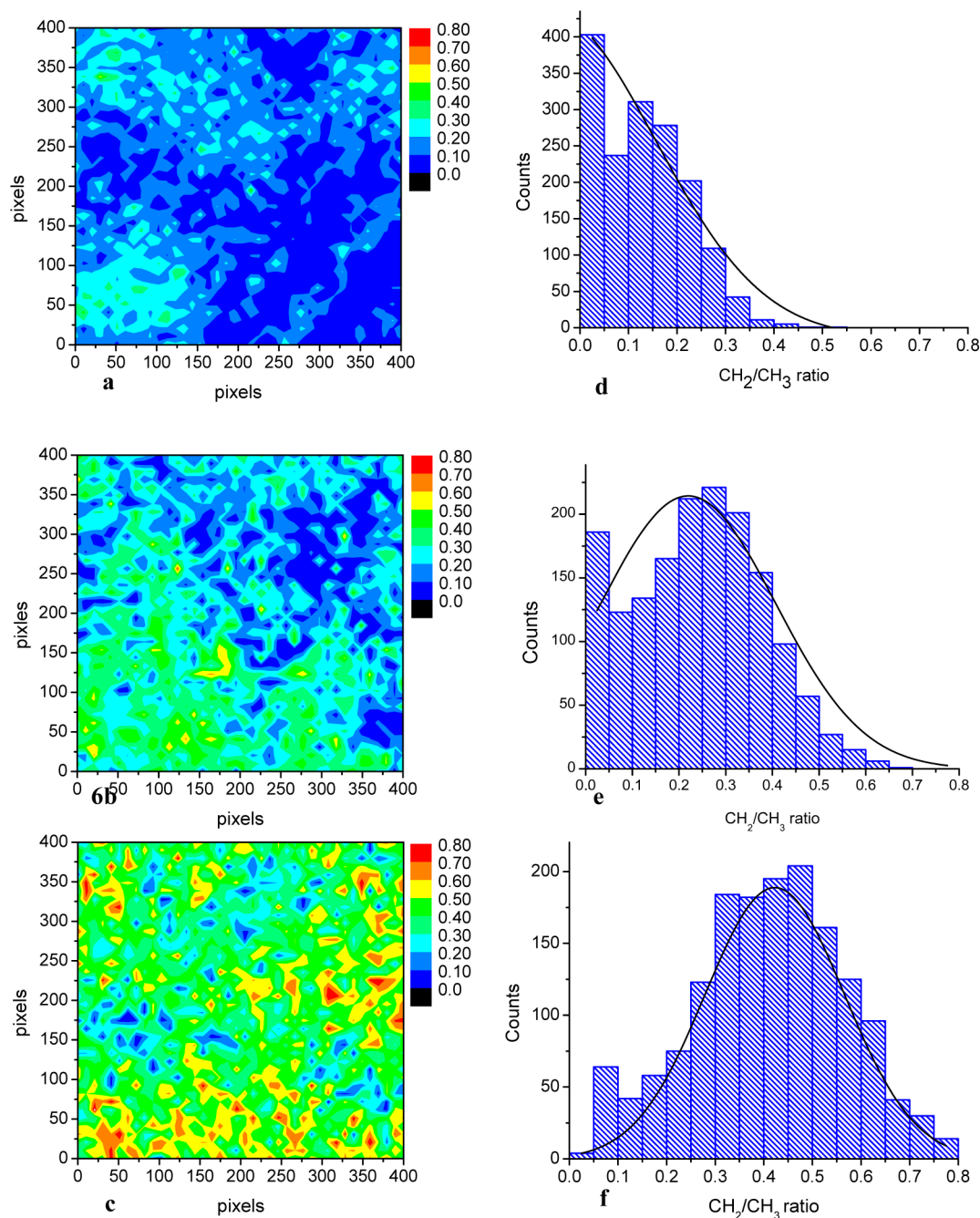


**Figure 7.** Contour plots of  $(d^+/r^+)$  ratio of SAMs derived from (a) R1ArMT, (b) R2ArMT, and (c) R3ArMT with their corresponding histogram plots (d–f, respectively).

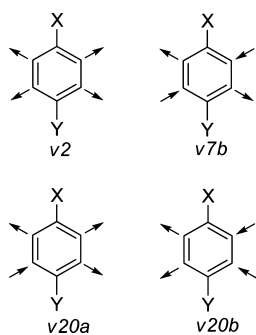


**Figure 8.** Aromatic stretching C–H modes.

of the surface, we used SFG-IM to scan the monolayers. SFG spectroscopy, though a surface-sensitive process, shows only the average spectra of the SAMs of a 1 mm area of the substrate, the typical laser spot size. Because only the average spectra is analyzed, there is a bias for the regions of high order because their SFG signal would be much greater than that of disordered areas. SFG-IM can provide additional information on the spatial distribution of the methyl group orientations and the conformational order of the monolayers by accounting for the regions of lower orientation and conformational order. Each  $10 \times 10$  pixel ROI is analyzed independently and assigned a methyl group tilt angle based on the  $r^+/r^-$  ratio curve presented in Figure 5. This curve assumes a delta-function distribution for the methyl tilt angles, where all alkyl chains in

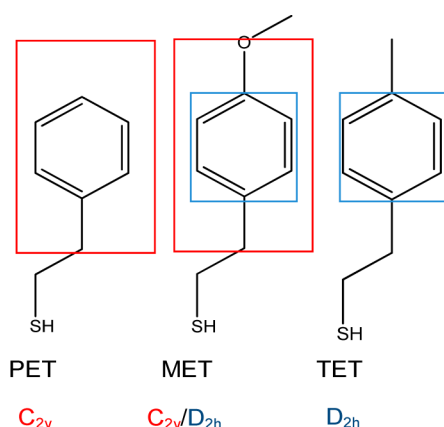


Figure 9. Proposed symmetries of the model phenylalkanethiols.

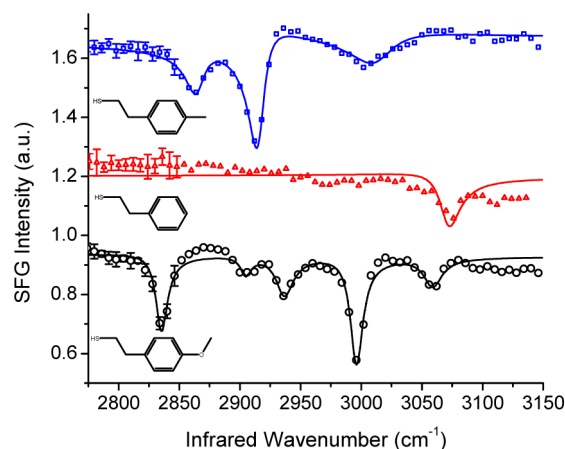


Figure 10. SFG spectra of SAMs derived from MET, PET, and TET on gold in the CH region.

given ROI assume the same tilt angle. The conformational order is estimated from the ratio of the methylene symmetric and the methyl symmetric C–H ( $d^+/r^+$ ) stretching modes. Furthermore, the distributions of methyl group tilt angles and  $d^+/r^+$  can be used to estimate the magnitude of the monolayer disorder by comparing the standard deviations of the distributions.

The calculated methyl tilt angles of each were remapped onto 2D contour plots along with the histograms showing the number of times the tilt angles occurred (Figure 6). A Gaussian distribution function was used to approximate the average and standard deviation of the tilt angles (Table 3). The methyl group tilt angles of the SAMs agree with the trend derived from

SFG spectroscopy:  $R1ArMT < R2ArMT < R3ArMT$ . The contour plots and the histograms show that the methyl tilt angles of the SAMs are homogeneous with a standard deviation of  $<6^\circ$ , suggesting that their conformational order is similar to SAMs derived from alkanethiols such as ODT.<sup>28</sup>

It is also interesting to compare the methyl group tilt angle distributions derived from SFG-IM with those obtained from the average spectra of a  $400 \times 400$  sample spot. In Figure 5, each curve shows a different distribution width and tilt angle range based on the Gaussian distribution function. At  $\sigma = 0^\circ$ , the delta function assumes that all alkyl chains will have the same tilt angles, which is not a reasonable assumption.  $R1ArMT$ , which has an average  $(r^+/r^-)^2$  of 2.0, is estimated to have tilt angles/distribution width pairs:  $(33^\circ, \sigma = 0^\circ)$ ,  $(28^\circ, \sigma = 10^\circ)$ , and  $(24^\circ, \sigma = 20^\circ)$ . Similarly, at distribution widths ranging from 0 to  $20^\circ$ ,  $R2ArMT$  and  $R3ArMT$  have a methyl group tilt angle ranging from 37 to  $41^\circ$  and 42 to  $50^\circ$ , respectively. However, these methyl group tilt angles and distribution widths do not necessarily reflect actual values. A previous SFG-IM study has shown that distributions obtained from large ROIs tend to favor tilt angles of  $40\text{--}60^\circ$ .<sup>28,44</sup> Methyl tilt angles outside this range have lower SFG intensities and thus are not detected.<sup>28</sup> The advantage of SFG-IM is that it can experimentally determine the distribution by extracting the methyl group tilts angles from small ROIs independently, thus accounting for the less favorable molecular arrangements, and provide a better interpretation of the surface.

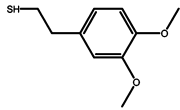
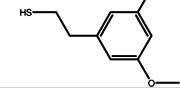
The chain density of the  $R1ArMT$  SAM is lower than that of SAMs derived from alkanethiols such as ODT due to the void space created by the volume dissimilarity between the alkoxy chain and the benzene ring. The diminished van der Waals interactions lead to diminished conformational order. For  $R2ArMT$ , the two alkoxy chains on the meta carbons of the aromatic ring might force the alkoxy chains to twist and kink until the methylene groups nearer the surface are able to form all-trans conformations. The  $R3ArMT$  SAM experiences additional disorder from the three alkoxy chains on the benzene ring. The para alkoxy chain is significantly different with the ones connected to the meta carbons in terms of height and tilt angle. All of these factors can introduce defects in the monolayer and decrease its conformational order. However, the standard deviation of the methyl group tilts (Table 3) shows no significant increase in conformational order, implying that the methylene groups near the aromatic ring might kink and twist, but nearer the surface, the chains align to form all-trans conformations.

Gauche defects near the monolayer–air interface can be indirectly measured using contact-angle experiments. Previous

Table 4. Vibrational Assignments of SAMs Derived from PET, MET, and TET

| Compound | Wavenumber( $cm^{-1}$ ) | Vibrational assignment   |
|----------|-------------------------|--|
| PET      | 3070                    | aromatic $\nu_2$ C–H stretch   |
| MET      | 2835                    | methoxy out of plane CH stretch $\nu_s CH_{2(out)}$ <sup>47,48</sup> |
|          | 2904                    | $CH_3$ bending mode overtone <sup>48</sup>                           |
|          | 2936                    | $\nu_{as} CH_{2(out)}$ stretch <sup>48</sup>                         |
|          | 2999                    | $\nu CH_{(in)}$ <sup>48</sup>  |
| TET      | 3058                    | aromatic $\nu_2$ CH stretch  |
|          | 2871                    | In phase methyl symmetric stretch                                    |
|          | 2927                    | methyl symmetric stretch Fermi resonance                             |
|          | 3003                    | methyl asymmetric stretch  |

Table 5. Vibrational Assignments of SAMs Derived from 3,4-DMP and 3,5-DMP

| Compound   | Wavenumber( $\text{cm}^{-1}$ ) | Vibrational assignment  |
|--|--------------------------------|---|
| <br>3,4-DMP | 2835                           | methoxy out of plane CH stretch $\nu_s\text{CH}_2(\text{out})$ <sup>47,48</sup> |
|  | 2907                           | $\text{CH}_3$ bending mode overtone <sup>48</sup>                               |
|  | 2936                           | $\nu_{\text{as}}\text{CH}_2(\text{out})$ stretch <sup>48</sup>                  |
|  | 3000                           | $\nu\text{CH}(\text{in})$ <sup>48</sup>   |
| <br>3,5-DMP | 2837                           | methoxy out of plane CH stretch $\nu_s\text{CH}_2(\text{out})$ <sup>47,48</sup> |
|  | 2914                           | $\text{CH}_3$ bending mode overtone <sup>48</sup>                               |
|  | 2936                           | $\nu_{\text{as}}\text{CH}_2(\text{out})$ stretch <sup>48</sup>                  |
|  | 3002                           | $\nu\text{CH}(\text{in})$ <sup>48</sup>   |

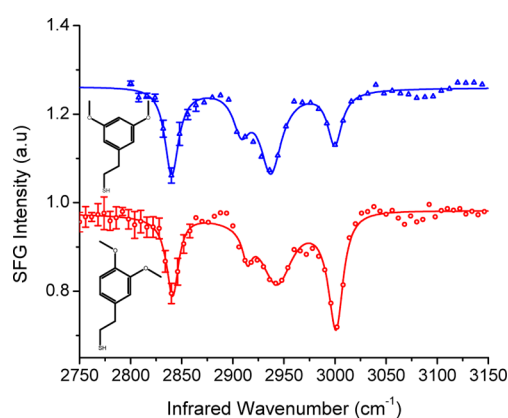


Figure 11. SFG spectra of SAMs derived from 3,5-DMP (top) and 3,4-DMP (bottom) SAMs in the CH region on gold slides immersed in 1 mM solution of thiols.

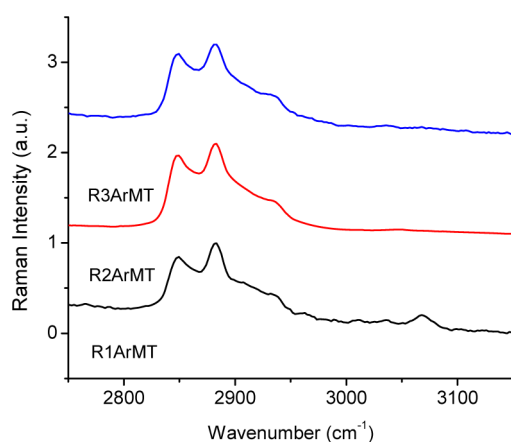


Figure 12. Raman spectra of R1ArMT, R2ArMT, and R3ArMT.

studies have reported that gauche defects that expose the methylene groups at the interface can cause a methyl-terminated SAM to become more wettable.<sup>2,3</sup> Rittikulsittichai et al. reported the trend of the hexadecane and decalin contact angles of the studied SAMs to be as follows:  $\text{ODT} \sim \text{R1ArMT} > \text{R3ArMT} \gg \text{R2ArMT}$ ,<sup>20</sup> which implies that the R1ArMT monolayer has a similar conformational order as ODT, followed closely by R3ArMT, while the SAM derived from R2ArMT proved to be the least ordered of the monolayers. Comparing the degree of film order of these SAMs based on the relative intensity of  $d^+/r^+$ , Figure 7 shows that the R1ArMT SAM has weak methylene resonances and the methylene

resonances of the R2ArMT and R3ArMT SAMs are significantly stronger. For R2ArMT, the two alkoxy chains are attached to the meta positions of the aromatic ring, leaving the para position unoccupied. The kinking and twisting of the alkoxy chains might be insufficient to overcome the disorder caused by this void space. This conformational disorder leads to gauche defects in the R2ArMT SAM, which are detectable in both SFG and contact-angle measurements.

For the R3ArMT SAM, however, the methylene gauche defects observed by SFG were undetectable in contact-angle measurements using nonpolar probe liquids (e.g., hexadecane). Contact angles are particularly sensitive to gauche defects near the surface, such as those commonly found in loosely packed monolayers. The methylene resonances from the R3ArMT SAM might arise from kink defects where the alkoxy chains are attached to the phenyl ring, undetectable by contact-angle measurements but visible to SFG spectroscopy. Tillman and coworkers<sup>41</sup> studied the incorporation of a phenoxy group into long-chain alkyltrichlorosilane SAMs and found that chains having eight or more carbon units above the ring would produce monolayers having contact angles similar to normal alkylsilane SAMs, suggesting that the addition of the third alkoxy chain at the para carbon reduces gauche defects near the surface by filling the void space and allowing the chains to align to form all-trans configurations. Table 3 shows that surface heterogeneity of the  $d^+/d^-$  increases as follows:  $\text{R1ArMT} < \text{R2ArMT} < \text{R3ArMT}$ , which also suggests that the conformational order decreases when additional alkoxy chains are attached to the benzene ring.

**4.4. Aromatic CH Stretch.** The resonance appearing at  $3070\text{ cm}^{-1}$  in both the ppp and ssp spectra of R1ArMT can be assigned as an aromatic in-phase C–H stretch  $\nu_2$ .<sup>38</sup> The identity of the resonance was in question because the SAMs derived from R2ArMT and R3ArMT exhibit no aromatic C–H resonances, and all three thiols possess a  $C_{2v}$  symmetry along the aromatic ring that allows phenyl C–H stretching modes to be SFG-active. However, only the R1ArMT SAMs exhibit this dip. Nishi and coworkers, when analyzing *o*-, *p*-, and *m*-methyl phenylmethanethiol SAMs on gold, observed no resonances in this region.<sup>45</sup> Bell et al., in their analysis of phenyltosylates, found that the *p*-disubstituted aromatic compounds having  $C_{2v}$  symmetry had a resonance at  $3057\text{ cm}^{-1}$ , which they assigned as the combination of the  $\nu_2$  modes and  $\nu_{20b}$ , and a dip at  $3021\text{ cm}^{-1}$ , assigned as  $\nu_{20a}$ .<sup>39</sup> Figure 8 shows these normal-mode assignments.

It is plausible that the aromatic C–H modes of R1ArMT are SFG-active due to local  $C_{2v}$  symmetry at the aromatic ring. To test this hypothesis, we prepared several SAMs from 2-

phenylethanethiol (PET), 2-(4-methoxy-phenyl)ethanethiol (MET), and 2-*p*-tolyl-ethanethiol (TET) and analyzed them by SFG spectroscopy. PET was chosen because when it forms a monolayer, its aromatic ring has local  $C_{2v}$  symmetry (Figure 9) due to the different substituents attached to carbons 1 and 4. For TET, the methyl and ethyl groups attached to the first and fourth carbons, respectively, of the aromatic ring are sufficiently similar so that its local symmetry would be approximately  $D_{2h}$ . Because TET has a local center of inversion, its aromatic C–H modes would be SFG-inactive. MET should either have a  $C_{2v}$  or  $D_{2h}$  symmetry. If the methoxy group is sufficiently different from the ethyl group at the para position, then the MET molecule should possess  $C_{2v}$  symmetry and exhibit an aromatic C–H stretching resonance. Otherwise, MET would have  $D_{2h}$  symmetry.

Figure 10 shows that the SFG spectrum of the SAMs derived from PET exhibits a dip at  $3070\text{ cm}^{-1}$ , which is assigned to  $\nu_2$ , the aromatic ring C–H stretching mode (Table 4). In contrast, SAMs derived from TET exhibit the  $r^+$  and  $r^{\text{FR}}$  modes (Fermi resonance with the  $\text{CH}_3$  deformation overtone), but the  $r^-$  mode is noticeably absent due to its low IR intensity and low Raman cross-section.<sup>45,46</sup> The spectrum of the SAMs derived from MET exhibits aromatic C–H stretches modes at  $3013$  and  $3077\text{ cm}^{-1}$ . The results agree with the hypothesis that PET having a  $C_{2v}$  symmetry, would have SFG-active aromatic C–H modes, while TET, having  $D_{2h}$  symmetry would not. MET and consequently R1ArMT, also have  $C_{2v}$  symmetries because their aromatic stretching modes are SFG-active.

Thus, the  $C_{2v}$  symmetry of R1ArMT allows its aromatic C–H stretches, which have  $A_1$  symmetry, to be SFG-active. Also, the presence of this aromatic stretching mode shows that the aromatic ring is oriented nearly perpendicular to the surface. It can then be inferred that the aromatic ring of the R1ArMT monolayer is oriented along the surface normal. In contrast, the R2ArMT and R3ArMT monolayers exhibit no aromatic C–H stretching modes in their SFG spectra. It is possible that the long alkoxy chains affect the orientation of the benzene rings, decreasing the aromatic stretching mode intensities. If this phenomenon is at play, then short methoxy groups attached to the benzene ring should not significantly affect its orientation, and aromatic stretching modes should appear in the SFG spectra. 2-(3,4-Dimethoxyphenyl)ethanethiol (3,4-DMP) was synthesized and analyzed to test this hypothesis (Table 5). 2-(3,5-Dimethoxyphenyl)ethanethiol (3,5-DMP) was also synthesized and analyzed because it has no plane of symmetry perpendicular to ring plane, and its aromatic C–H stretching modes should be SFG-active. As shown by Figure 11, both thiols show methoxy resonances but no aromatic stretching modes, which suggests that the long alkoxy chains did not cause the SFG inactivity of the aromatic C–H stretching modes by altering the orientation of the benzene ring. The lack of aromatic C–H resonances in 3,5-DMP spectra also suggests that the symmetry of R2ArMT and R3ArMT was not the reason why these two thiol adsorbates exhibit no aromatic resonances in SFG.

Further information could be gleaned from Raman spectroscopy studies of the phenylalkanethiols (Figure 12). As shown in the Raman spectra, only R1ArMT has a peak in the aromatic CH region, whereas R2ArMT and R3ArMT have Raman contributions only from aliphatic CH stretching modes. It has been observed that electron-donating groups (EDGs), such as alkoxy groups, reduce the aromatic C–H Raman intensities significantly.<sup>49</sup> The addition of two or more EDGs on the

aromatic rings might cause the R2ArMT and R3ArMT aromatic rings to exhibit weak Raman intensities, which might rationalize why both corresponding monolayers exhibit no aromatic stretching modes in SFG.

## 5. CONCLUSIONS

SAMs formed by the alkoxyphenylethanethiols, R1ArMT, R2ArMT, and R3ArMT, were found to be well-ordered with gauche and kink defects. These defects were caused by the cross-sectional difference of the alkoxy chains and the aromatic ring, forcing the chains to tilt and kink until the methylene groups further above the chains could align to form the all-trans conformation. Orientation analyses show that methyl group tilt increases as the number of alkoxy chains attached to the aromatic ring is increased, implying that conformational order is reduced due to steric effects. By analyzing several model phenylethylthiols with different symmetries along the aromatic ring, it was confirmed that R1ArMT exhibits an aromatic C–H stretch. The SFG spectra of SAMs of PET, MET, and TET suggest that phenylethanethiols form closely packed monolayers with the benzene rings oriented along the surface normal. Analysis of 3,4-DMP and 3,5-DMP suggests that the R2ArMTs and R3ArMT's lack of SFG-active aromatic resonances was not due to changes in the orientation caused by long alkoxy chains nor was it due to symmetry. Raman data suggest that the electron-withdrawing alkoxy groups decreased the Raman cross section, which in turn weakened the SFG intensity of the aromatic C–H stretching resonances.

## AUTHOR INFORMATION

### Corresponding Author

\*E-mail: trlee@uh.edu (T.R.L.); sbaldelli@uh.edu (S.B.).

### Notes

The authors declare no competing financial interest.

## ACKNOWLEDGMENTS

We are grateful for generous financial support from the National Science Foundation (DMR-0856009 and DMR-0906727), the Robert A. Welch Foundation (E-1320), and the Texas Center for Superconductivity at the University of Houston. We also thank Zlata Grenoble for the Raman spectroscopy of the phenylethanethiols.

## REFERENCES

- (1) Shon, Y.-S.; Colorado, R., Jr.; Williams, C. T.; Bain, C. D.; Lee, T. R. Low-Density Self-Assembled Monolayers on Gold Derived from Chelating 2-Monoalkylpropane-1,3-Dithiols. *Langmuir* **2000**, *16*, 541–548.
- (2) Shon, Y.-S.; Lee, T. R. Chelating Self-Assembled Monolayers on Gold Generated from Spiroalkanedithiols. *Langmuir* **1999**, *15*, 1136–1140.
- (3) Park, J.-S.; Vo, A. N.; Barriet, D.; Shon, Y.-S.; Lee, T. R. Systematic Control of the Packing Density of Self-Assembled Monolayers Using Bidentate and Tridentate Chelating Alkanethiols. *Langmuir* **2005**, *21*, 2902–2911.
- (4) Garg, N.; Lee, T. R. Self-Assembled Monolayers Based on Chelating Aromatic Dithiols on Gold. *Langmuir* **1998**, *14*, 3815–3819.
- (5) Bain, C. D.; Troughton, E. B.; Tao, Y. T.; Evall, J.; Whitesides, G. M.; Nuzzo, R. G. Formation of Monolayer Films by the Spontaneous Assembly of Organic Thiols from Solution onto Gold. *J. Am. Chem. Soc.* **1989**, *111*, 321–335.
- (6) Yu, B.; Qian, L.; Yu, J.; Zhou, Z. Effects of Tail Group and Chain Length on the Tribological Behaviors of Self-Assembled Dual-Layer Films in Atmosphere and in Vacuum. *Tribol. Lett.* **2009**, *34*, 1–10.

- (7) Zhang, S.; Jamison, A. C.; Schwartz, D. K.; Lee, T. R. Self-Assembled Monolayers Derived from a Double-Chained Monothiol Having Chemically Dissimilar Chains. *Langmuir* **2008**, *24*, 10204–10208.
- (8) Cimatu, K.; Moore, H. J.; Barriet, D.; Chinwangso, P.; Lee, T. R.; Baldelli, S. Sum Frequency Generation Imaging Microscopy of Patterned Self-Assembled Monolayers with Terminal -CH<sub>3</sub>, -OCH<sub>3</sub>, -CF<sub>2</sub>CF<sub>3</sub>, -C≡C-, -Phenyl, and -Cyclopropyl Groups. *J. Phys. Chem. C* **2008**, *112*, 14529–14537.
- (9) Wenzl, I.; Yam, C. M.; Barriet, D.; Lee, T. R. Structure and Wettability of Methoxy-Terminated Self-Assembled Monolayers on Gold. *Langmuir* **2003**, *19*, 10217–10224.
- (10) Colorado, R., Jr.; Lee, T. R. Wettabilities of Self-Assembled Monolayers on Gold Generated from Progressively Fluorinated Alkanethiols. *Langmuir* **2003**, *19*, 3288–3296.
- (11) Lee, S.; Puck, A.; Graupe, M.; Colorado, R., Jr.; Shon, Y.-S.; Lee, T. R.; Perry, S. S. Structure, Wettability, and Frictional Properties of Phenyl-Terminated Self-Assembled Monolayers on Gold. *Langmuir* **2001**, *17*, 7364–7370.
- (12) Shon, Y.-S.; Kelly, K. F.; Halas, N. J.; Lee, T. R. Fullerene-Terminated Alkanethiolate Sams on Gold Generated from Unsymmetrical Disulfides. *Langmuir* **1999**, *15*, 5329–5332.
- (13) Nuzzo, R. G.; Dubois, L. H.; Allara, D. L. Fundamental Studies of Microscopic Wetting on Organic Surfaces. I. Formation and Structural Characterization of a Self-Consistent Series of Polyfunctional Organic Monolayers. *J. Am. Chem. Soc.* **1990**, *112*, 558–569.
- (14) Evans, S. D.; Urankar, E.; Ulman, A.; Ferris, N. Self-Assembled Monolayers of Alkanethiols Containing a Polar Aromatic Group: Effects of the Dipole Position on Molecular Packing, Orientation, and Surface Wetting Properties. *J. Am. Chem. Soc.* **1991**, *113*, 4121–4131.
- (15) Ulman, A. Formation and Structure of Self-Assembled Monolayers. *Chem. Rev.* **1996**, *96*, 1533–1554.
- (16) Love, J. C.; Estroff, L. A.; Kriebel, J. K.; Nuzzo, R. G.; Whitesides, G. M. Self-Assembled Monolayers of Thioliates on Metals as a Form of Nanotechnology. *Chem. Rev.* **2005**, *105*, 1103–1170.
- (17) Dubois, L. H.; Zegarski, B. R.; Nuzzo, R. G. Molecular Ordering of Organosulfur Compounds on Au(111) and Au(100): Adsorption from Solution and in Ultrahigh Vacuum. *J. Chem. Phys.* **1993**, *98*, 678–688.
- (18) Dubois, L. H.; Nuzzo, R. G. Synthesis, Structure, and Properties of Model Organic Surfaces. *Annu. Rev. Phys. Chem.* **1992**, *43*, 437–463.
- (19) Shon, Y.-S.; Colorado, R.; Williams, C. T.; Bain, C. D.; Lee, T. R. Low-Density Self-Assembled Monolayers on Gold Derived from Chelating 2-Monoalkylpropane-1,3-Dithiols. *Langmuir* **1999**, *16*, 541–548.
- (20) Rittikulsittichai, S.; Jamison, A. C.; Lee, T. R. Self-Assembled Monolayers Derived from Alkoxyphenylethanethiols Having One, Two, and Three Pendant Chains. *Langmuir*, *27*, 9920–9927.
- (21) Evans, S. D.; Urankar, E.; Ulman, A.; Ferris, N. Self-Assembled Monolayers of Alkanethiols Containing a Polar Aromatic Group: Effects of the Dipole Position on Molecular Packing, Orientation, and Surface Wetting Properties. *J. Am. Chem. Soc.* **1991**, *113*, 4121–4131.
- (22) Bain, C. D. Sum-Frequency Vibrational Spectroscopy of the Solid/Liquid Interface. *J. Chem. Soc., Faraday Trans.* **1995**, *91*, 1281–1296.
- (23) Buck, M.; Himmelhaus, M. Vibrational Spectroscopy of Interfaces by Infrared-Visible Sum Frequency Generation. *J. Vac. Sci. Technol., A* **2001**, *19*, 2717–2736.
- (24) Bain, C. D.; Davies, P. B.; Ong, T. H.; Ward, R. N.; Brown, M. A. Quantitative Analysis of Monolayer Composition by Sum-Frequency Vibrational Spectroscopy. *Langmuir* **1991**, *7*, 1563–1566.
- (25) Ward, R. N.; Davies, P. B.; Bain, C. D. Orientation of Surfactants Adsorbed on a Hydrophobic Surface. *J. Phys. Chem.* **1993**, *97*, 7141–7143.
- (26) Duffy, D. C.; Davies, P. B.; Bain, C. D. Surface Vibrational Spectroscopy of Organic Counterions Bound to a Surfactant Monolayer. *J. Phys. Chem.* **1995**, *99*, 15241–15246.
- (27) Zhang, H.; Romero, C.; Baldelli, S. Preparation of Alkanethiol Monolayers on Mild Steel Surfaces Studied with Sum Frequency Generation and Electrochemistry. *J. Phys. Chem. B* **2005**, *109*, 15520–15530.
- (28) Cimatu, K.; Baldelli, S. Spatially Resolved Surface Analysis of an Octadecanethiol Self-Assembled Monolayer on Mild Steel Using Sum Frequency Generation Imaging Microscopy. *J. Phys. Chem. C* **2007**, *111*, 7137–7143.
- (29) Hernandez, M.; Chinwangso, P.; Cimatu, K.; Srisombat, L. O.; Lee, T. R.; Baldelli, S. Chemical Imaging and Distribution Analysis of Mono-, Bi-, and Tridentate Alkanethiol Self-Assembled Monolayers on Gold by Sum Frequency Generation Imaging Microscopy. *J. Phys. Chem. C* **2011**, *115*, 4688–4695.
- (30) Schneider, C. A.; Rasband, W. S.; Eliceiri, K. W. NIH Image to ImageJ: 25 Years of Image Analysis. *Nat. Methods* **2012**, *9*, 671–675.
- (31) Hirose, C.; Yamamoto, H.; Akamatsu, N.; Domen, K. Orientation Analysis by Simulation of Vibrational Sum Frequency Generation Spectrum: CH Stretching Bands of the Methyl Group. *J. Phys. Chem.* **1993**, *97*, 10064–10069.
- (32) Hirose, C.; Akamatsu, N.; Domen, K. Formulas for the Analysis of Surface Sum-Frequency Generation Spectrum by CH Stretching Modes of Methyl and Methylene Groups. *J. Chem. Phys.* **1992**, *96*, 997–1004.
- (33) Wang, H.-F.; Gan, W.; Lu, R.; Rao, Y.; Wu, B.-H. Quantitative Spectral and Orientational Analysis in Surface Sum Frequency Generation Vibrational Spectroscopy (Sfg-Vs). *Int. Rev. Phys. Chem.* **2005**, *24*, 191–256.
- (34) MacPhail, R. A.; Strauss, H. L.; Snyder, R. G.; Elliger, C. A. Carbon-Hydrogen Stretching Modes and the Structure of N-Alkyl Chains. 2. Long, All-Trans Chains. *J. Phys. Chem.* **1984**, *88*, 334–341.
- (35) Snyder, R. G. Group Moment Interpretation of the Infrared Intensities of Crystalline N-Paraffins. *J. Chem. Phys.* **1965**, *42*, 1744–1763.
- (36) Snyder, R. G.; Strauss, H. L.; Elliger, C. A. Carbon-Hydrogen Stretching Modes and the Structure of N-Alkyl Chains. 1. Long, Disordered Chains. *J. Phys. Chem.* **1982**, *86*, 5145–5150.
- (37) Tuccitto, N.; Ferri, V.; Cavazzini, M.; Quici, S.; Zhavnerko, G.; Licciardello, A.; Rampi, M. A. Highly Conductive [Sim]40-nm-Long Molecular Wires Assembled by Stepwise Incorporation of Metal Centres. *Nat. Mater.* **2009**, *8*, 41–46.
- (38) Wilson, E. B. The Normal Modes and Frequencies of Vibration of the Regular Plane Hexagon Model of the Benzene Molecule. *Phys. Rev.* **1934**, *45*, 706.
- (39) Bell, G. R.; Li, Z. X.; Bain, C. D.; Fischer, P.; Duffy, D. C. Monolayers of Hexadecyltrimethylammonium P-Tosylate at the Air-Water Interface. 1. Sum-Frequency Spectroscopy. *J. Phys. Chem. B* **1998**, *102*, 9461–9472.
- (40) Guyot-Sionnest, P.; Hunt, J. H.; Shen, Y. R. Sum-Frequency Vibrational Spectroscopy of a Langmuir Film: Study of Molecular Orientation of a Two-Dimensional System. *Phys. Rev. Lett.* **1987**, *59*, 1597.
- (41) Tillman, N.; Ulman, A.; Schildkraut, J. S.; Penner, T. L. Incorporation of Phenoxy Groups in Self-Assembled Monolayers of Trichlorosilane Derivatives. Effects on Film Thickness, Wettability, and Molecular Orientation. *J. Am. Chem. Soc.* **1988**, *110*, 6136–6144.
- (42) Tao, F.; Bernasek, S. L. Understanding Odd-Even Effects in Organic Self-Assembled Monolayers. *Chem. Rev.* **2007**, *107*, 1408–1453.
- (43) Naoya, N.; Daisuke, H.; Masahiro, Y.; Takashi, K. Chain-Length-Dependent Change in the Structure of Self-Assembled Monolayers of N-Alkanethiols on Au(111) Probed by Broad-Bandwidth Sum Frequency Generation Spectroscopy. *J. Chem. Phys.* **2003**, *118*, 1904–1911.
- (44) Santos, G.; Baldelli, S. Scale Dependence of the Orientation and Conformation Distribution Analysis of a Molecular Monolayer Using Sum Frequency Generation Imaging Microscopy. *J. Phys. Chem. C* **2012**, *116*, 25874–25887.
- (45) Nishi, N.; Hobar, D.; Yamamoto, M.; Kakiuchi, T. Orientation of O-, M-, and P-Methylbenzylmercaptans Adsorbed on Au(111) Probed by Broad-Bandwidth Sum Frequency Generation Spectroscopy. *Langmuir* **2003**, *19*, 6187–6192.

(46) Tao, Y.; Wu, C.; Eu, J.; Lin, W.; Wu, K.; Chen, C. Structure Evolution of Aromatic-Derivatized Thiol Monolayers on Evaporated Gold. *Langmuir* **1997**, *13*, 4018–4023.

(47) Colthup, N. B.; Daly, L. H.; Wiberley, S. E. *Introduction to Infrared and Raman Spectroscopy*, 3rd ed.; American Press: San Diego, CA, 1990.

(48) Ong, T. H.; Davies, P. B.; Bain, C. D. Sum-Frequency Spectroscopy of Monolayers of Alkoxy-Terminated Alkanethiols in Contact with Liquids. *Langmuir* **1993**, *9*, 1836–1845.

(49) Venkateswarlu, K.; Radhakrishnan, M. Study of the Electrical Nature of Some Atoms and Groups from Raman Effect. *Spectrochim. Acta* **1962**, *18*, 1433–1439.